Chemical Geology 636 (2023) 121651

Contents lists available at ScienceDirect

Chemical Geology

journal homepage: www.elsevier.com/locate/chemgeo

In situ S isotopic analysis in apatite using laser ablation-multiple collector-inductively coupled plasma mass spectrometry

Qinglin Li [a], Wen Zhang [a,*], Zhaochu Hu [a], Yantong Feng [b], Hao Hu [a], Tao Luo [a], Jing Huang [a], Xianli Zeng [a]

[a] *State Key Laboratory of Geological Processes and Mineral Resources, China University of Geosciences, Wuhan 430074, China*
[b] *Gansu Key Laboratory of Mineral Resources in Western China, School of Earth Sciences, Lanzhou University, Lanzhou 730000, China*

ARTICLE INFO

Editor: S Aulbach

Keywords:
S isotope analysis
Apatite
LA-MC-ICP-MS
Reference materials

ABSTRACT

The S isotope composition ($^{34}S/^{32}S$) in apatite has been considered as a new powerful tool to trace S source reservoirs and to evaluate redox state and dynamic sulfur behavior in magmatic systems. This study presents the first *in situ* method to analyze S isotope compositions in apatite using laser ablation multiple collector inductively coupled plasma mass spectrometry (LA-MC-ICP-MS). The sulfur isotope analysis of low-S apatite suffered the problem of high background interference, resulting in a low ratio of signal to noise (S/N). A detailed investigation found that ~50% background of S isotopes originated from memory effect in the aerosol particles transformation system and can be removed through careful cleaning or replacement. A linear regression calculation method was proposed instead of the traditional data reduction method to improve the performance of correcting the S background signal. Femtosecond laser ablation system (fs-LA) was used to reduce the thermal effect and suppress the potential fractionation of S isotopes during the laser ablation process, significantly improving the stability of $\delta^{34}S_{V\text{-}CDT}$ values at different laser ablation parameters. Seven natural apatite samples with a large S concentration range were measured by the presented method. A good agreement of $\delta^{34}S_{V\text{-}CDT}$ values between fs-LA-MC-ICP-MS and IR-MS was obtained. The reproducibility of $\delta^{34}S_{V\text{-}CDT}$ obtained from fs-LA-MC-ICP-MS was similar to that in SIMS. These results confirm that the presented method can provide high-quality S isotopic compositions in natural apatites. Four apatite samples (Sly-1, Sly-2, MG, and OL-1) with various concentrations of SO_3 (0.21% to 1.26%) show the homogeneous S isotope compositions based on the large amounts of repeated analyses using fs-LA-MC-ICP-MS. They are suggested as the high-quality external reference materials for *in situ* S isotope analysis for LA-MC-ICP-MS and SIMS.

1. Introduction

Apatite [$Ca_5(PO_4)_3(F,Cl,OH)$] is a common accessory mineral in igneous, metamorphic and clastic sedimentary rocks and one of the important carrying minerals for volatiles, rare earth elements (REEs), phosphorus, strontium and notable quantities of uranium and thorium (Piccoli et al., 2002; Webster et al., 2015). These elements mainly enter the apatite lattice through various substitution models, and their concentration in apatite is depend on magma composition, magma differentiation, temperature and pressure and oxygen fugacity (Piccoli et al., 2002; Jennings et al., 2011; Parat et al., 2011; Li and Zhou, 2015). Geochemical information of apatite hence has been widely used to trace magma source and evolutionary processes, such as the crystallization process and crystallization environment in magma chamber (Dempster et al., 2003; Zirner et al., 2015), the effect of volatile components on magmatic-hydrothermal processes (Doherty et al., 2014; Palma et al., 2019), the source of the magmas and as a tracer of the evolving hydrothermal fluids using Sr, Nd and O isotopes (Rakovan et al., 1997; Li and Zhou, 2015; Zeng et al., 2016), the reductive state and oxidation condition of the parental magma (Belousova et al., 2002; Miles et al., 2014), radiometric and fission track dating (Hasebe et al., 2004; Chew and Spikings, 2021).

Apatite can incorporate sulfur as sulfate (S^{6+}) to record sulfur activity in magmatic systems (Parat et al., 2002; Parat and Holtz, 2004; Parat and Holtz, 2005; Parat et al., 2011). Recent studies have shown that apatite also can incorporate S^{2-}, S^{4+} and S^{6+} in varying proportions as a function of fO_2 (Konecke et al., 2017; Brounce et al., 2019; Konecke et al., 2019; Sadove et al., 2019), revealing the potential to use the

---

* Corresponding author.
E-mail address: tuyaken@hotmail.com (W. Zhang).

https://doi.org/10.1016/j.chemgeo.2023.121651
Received 9 May 2023; Received in revised form 31 July 2023; Accepted 2 August 2023
Available online 3 August 2023

oxidation state of S in apatite to examine the evolution of redox conditions of magmatic systems. Moreover, S isotopic zoning (δ^{34}S) in apatite crystal has been reported through the micro-analytical method. Economos et al. (2017) developed the first *in situ* method of analyzing S isotopic ratios in apatite using secondary ion mass spectrometry (SIMS) and reported a large δ^{34}S fractionation of up to 6‰ from a single hand sample and up to 3.8‰ in a single crystal. These large δ^{34}S fractionations were attributed to degassing and mixing during the magmatic process in the open system, or the effect of anhydrite crystallization. Hammerli et al. (2021) further optimized SIMS technique for determining multiple S isotopes in apatite (δ^{34}S and δ^{33}S). Four apatite crystals were characterized and recommended as the reference materials for SIMS S isotope analysis (Hammerli et al., 2021). Kennedy et al. (2023) also reported twelve apatite samples as SIMS reference materials for U—Pb dating, Sr and S isotope analyses. The homogenous distribution of S isotope composition in eight apatites were observed. The S isotopes analysis using SIMS can provide high spatial resolution (15–20 μm), good analytical precision (~0.5‰ for δ^{34}S) and multiple S isotopes information, which support the application of S isotope in apatite to trace S source reservoirs and to track the pathway of magmatic-hydrothermal fluids in a wide range of geological settings.

LA-MC-ICP-MS (laser ablation multiple collector-inductively coupled plasma mass spectrometry) is also a main *in situ* technique for sulfur isotope measurement and focuses on sulfide and sulfate minerals, such as pyrite, chalcopyrite, sphalerite, barite, anhydrite. Mason et al. (2006) reported a pioneering work on sulfur isotope analysis using LA-MC-ICP-MS with large spot size (80–100 μm) and slightly high precision of δ^{34}S and δ^{33}S (0.6‰ and 1.5‰, respectively). The further works mainly investigated the matrix effects of different sulfide phases, the optimization of laser ablation parameters (laser fluence), the optimization of laser ablation strategies (spot mode *vs* scan mode), and the methods to overcome the polyatomic interferences. Fu et al. (2017) reported accurate determination of S isotopes in sulfides by femtosecond (fs)-LA-MC-ICP-MS with non-matrix matched calibration. Authors found that higher sensitivity, less matrix effect and more stable transient isotopic ratios were obtained when fs laser system was used to replace the nanosecond (ns) laser system. LA-MC-ICP-MS technique has so far been able to determine sulfur isotope ratios in various sulfides with moderate laser spot sizes (30–50 μm) and good precisions (~0.3‰ and ~ 0.6‰ for δ^{34}S and δ^{33}S, respectively). The advantages of LA-MC-ICP-MS are weaker matrix effects, more analyzable materials and cheaper instruments relative to SIMS. Therefore, LA-MC-ICP-MS is widely used in geochemical laboratories and provides micro-isotopic analysis services to geologists. However, LA-MC-ICP-MS have not been employed to measure the S isotope ratios for the low-S samples, such as apatites.

Here, we report the first *in situ* S isotope analysis method in natural apatite using LA-MC-ICP-MS. The high S background of MC-ICP-MS is an important factor affecting the analytical result of low-S minerals (such as apatite). We carefully investigated the background sources of S, evaluated the effect of data correction strategies on the data with the low ratio of signal to noise, and studied the effect of laser ablation parameters on isotope ratios. The S isotopic compositions of seven apatites are reported with good reproducibility comparable to that of SIMS. The *in situ* analysis results of the natural apatites are in good agreement with the recommended values measured by IRMS. Four natural apatite samples are proposed as potential reference materials for *in situ* analysis of S isotopes by LA-MC-ICP-MS and SIMS.

2. Experimental setup and analytical methods

2.1. Apatite samples

Seven natural apatites were used and analyzed in this study. Most apatites are *gem*-grade quality and purchased from world-wide gem merchants. LA-MC-ICP-MS generally has greater sample consumption in contrast to the high spatial analysis of SIMS. Therefore, the ideal natural reference materials for LA-MC-ICP-MS should be available in sufficient quantities to meet analytical consumption and be usable by the broader geological community. The investigated apatite samples in this study have large quantities from several grams to hundreds of grams (Table 1 and Fig. S1 in Supplement 1), which will serve the scientific community well over the long term.

The apatite of Sly-1 (5.68 g) and Sly-2 (14.50 g) which showed blue-green color and transparency, were from Irkutsk Oblast Lake Baikal area Slyudyanka, Russia. The apatite of MAD-1 (1.33 g), blue and pure crystal, was collected from Madagascar. The apatite of OL-1 (13.74 g) and OL-2 (374 g) come from Otter Lake, located in Quebec, Canada. They were green-yellow and opaque. The apatite of MG (44.79 g) was blue and translucent and from Minas Gerais State, Brazil. Durango apatite has been reported the S isotope composition by Economos et al. (2017) and Hammerli et al. (2021). Small amounts of Durango have been used in our lab for Sr isotope analysis and was also analyzed the S isotopic composition in this study. The relevant information is summarized in Table 1.

Apatite samples were crushed with a steel mortar to 1–2 mm size. Any fragments with visible imperfections under a binocular microscope were removed. The clean fragments were selected randomly (30–40 fragments for each sample) and embedded in epoxy resin and carefully polished to obtained flat surfaces for microscopic observation, major and trace elements analyses by EPMA and LA-ICP-MS, respectively, S isotope analyses by LA-MC-ICP-MS. Parts of the fragments were used for bulk analyses using isotope ratio mass spectrometry (IRMS).

2.2. Analytical techniques

2.2.1. In situ sulfur isotope analysis using LA-MC-ICP-MS

Micro-analysis of sulfur isotopes was performed on a NEPTUNE Plus MC-ICP-MS (Thermo Fisher Scientific, Bremen, Germany) combined with femtosecond laser system at GPMR Lab. The Neptune Plus, a double focusing MC-ICP-MS, was equipped with seven fixed electron multiplier ICs, and nine Faraday cups fitted with 10^{11} Ω resistors. In addition, a large dry interface pump (120 m^3 hr^{-1} pumping speed) and a X skimmer cone and Jet sample cone were used to increase the instrumental sensitivity. The Faraday collector configuration of the S isotope analysis was composed of an array of L2, C, H2 to monito ^{32}S, ^{33}S, ^{34}S. All measurements were performed in static mode using medium resolution with a resolving power of 5000 (peak edge width from 5% to 95% of the full peak height). The femtosecond laser ablation system is a NWR Femto^{UC} femtosecond system (New Wave Research, Fremont, CA, U.S.A.), which consisted of a 300 fs Yb:KGW femtosecond laser amplifier (PHAROS, Light Conversion Ltd., Vilnius, Lithuania) with a wavelength of 257 nm. The laser ablation was equipped with a two-volume cell (TV-2). Helium gas was filled into the ablation cell, while argon (~800 mL min^{-1}) and small amount of nitrogen (~4 mL min^{-1}) were mixed into the sample-out line downstream from the ablation chamber prior to entering the torch. A signal-smoothing device was used downstream from the sample cell.

Due to the low concentration of S in apatite, large laser spot sizes (50–60 μm), high frequency (50 Hz) and line scan mode were used in this study. The scan rate and laser fluence were fixed at 5 μm s^{-1} and ~ 3 J cm^{-2}. Individual data acquisition consisted of one block of 120 cycles with the integration time of 0.524 s per cycle. Total acquisition time for each measurement was approximately 62 s, including the 22 s of background signal following a time of 40 s for ablation signal acquisition. Therefore, each laser ablation analysis would produce a line of ~200 μm long and ~ 60 μm wide. Details of the instrumental operating conditions and measurement parameters are summarized in Table 2.

During the S isotope analysis using LA-MC-ICP-MS, most of interferences such as O-, N-, and H-based polyatomic species can be resolved through the high mass resolution power (Fu et al., 2016). But for apatites, the peak tailing of $^{35}Cl^{+}$ could be a potential mass spectrum interference on $^{34}S^{+}$ due to the high concentration of Cl in parts of

Table 1
Summary of samples and sample localities, and major element contents.

Sample name	Sample type	Sample mass (g)	Locality	CaO (%)	P_2O_5 (%)	SO_3 (%)	F (%)	Cl (%)
Sly-1	Apatite, crystal	5.68	Slyudyanka, Lake Baikal, Irkutskaya Oblast, Russia	54.62	41.76	1.21	2.43	0.09
Sly-2	Apatite, crystal	14.5	Slyudyanka, Lake Baikal, Irkutskaya Oblast, Russia	54.67	41.97	1.26	2.00	0.08
MAD-1	Apatite, crystal	1.33	Madagascar	53.50	40.43	0.93	2.96	0.24
OL-1	Apatite, crystal	13.74	Otter Lake, Outaouais, Canada	53.65	41.46	0.21	3.19	0.02
OL-2	Apatite, crystal	374	Otter Lake, Outaouais, Canada	53.98	40.82	0.34	2.59	0.02
MG	Apatite, crystal	44.79	Minas Gerais State, Brazil	54.88	40.67	1.17	1.92	0.36
Durango	Apatite, crystal	–	Mexico	54.20	41.05	0.41	3.31	0.43

Table 2
Instrumental set-up and operating conditions used in this study.

Mass spectrometer setup	
MC-ICP-MS	NEPTUNE Plus
RF power	1200 W
Cooling gas flow	16.0 L min^{-1}
Auxiliary gas flow	0.8–1.2 L min^{-1}
Sample gas flow	0.8–1.2 L min^{-1}
Cup configuration	L2(^{32}S), C(^{33}S), H2(^{34}S)
Interface cones	Jet sample cone+X skimmer cone
Acquisition mode	static
Instrument resolution	~5000 (media)
Electrode guard	Grounded
Block	1
Cycles /Block	120
Integration time	0.524 s.
Laser ablation system	
Laser type	NWR Femto^{UC} 257 nm
wavelength	257 nm
Carrier gas	He (0.50–0.66 L min^{-1})
Pulse length	300 fs
Spot diameter	60 μm
Laser frequency	50 Hz
Laser energy	~3 J cm^{-2}
Ablation mode	Line
Scan speed	5 μm s^{-1}

apatites (0.02–0.43 wt% in this study). We ablated a pressed pellet of NaCl (Cl = 60.66 wt%) to investigated the effect of the peak tailing of $^{35}Cl^+$. Fig. 1 shows the signal intensities from mass 31.5 to 35.5 when NaCl pellet was analyzed under medium resolution mode (~5000). No obvious signal interference between ^{34}S to ^{35}Cl was observed when the signal intensity of $^{35}Cl^+$ was up to 4 V. Therefore, the interference of the peak tailing of $^{35}Cl^+$ do not influence the mass of ^{34}S during the apatite analysis.

The other important interference was from the high signal of S isotopes in the background. A typical background signal of ^{32}S was about ~0.33 V in this study before optimization of instrument conditions, while the sample signals of ^{32}S in various apatites were from ~0.72 V to ~5.20 V. The ratio of signal to noise (S/N) of apatite analysis hence was from 2.2 to 15.8, which is much lower than that of sulfide analysis (S/N > 50 in pyrite analysis). The sources of S in the background were thought to from the working gases (Ar, He and N_2), entrained air, or residual sulfide at ablation cell, tube and ion extraction interface, *etc.* Gilbert et al. (2014) also found the signal of S isotopes in the background was effect by different tube materials. Here, a series of investigations was attempted to resolve the S background interference.

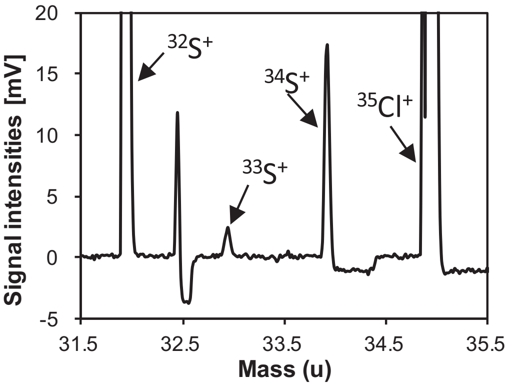

Fig. 1. The signal intensities from 31.5 to 35.5 when a NaCl pressed pellet was analyzed under medium resolution mode (~5000).

1. After cleaning the ablation cell, and replacing the new transmission tube, new sample cone, new skimmer cone, new torch (including the central tube), the S background signal can be reduced ~49%. Note that a new tube and a cone combination can reduced ^{32}S background by 29% and 22%, respectively. The results show that residual sulfur plays a significant role in the aerosol external transport system.
2. After replacing the new extraction lens (pure graphite) and new entrance slits (incident slit and slit tongue), no significant reduction of S background was observed, indicating that there are no large deposits of S ions in the interior of mass spectrum or the deposited ions are difficult to retransmit.
3. Two methods were used to purify the main working gases (Ar and He), cold trap and molecular sieve. We made a cold trap using stainless steel tube (1 m, 1/4 in. in diameter) and filled with stainless steel beads (1 mm in diameter) to improve temperature transmission efficiency. The steel tube was coiled, and then placed in liquid nitrogen (−196 °C) or a mixture of liquid nitrogen and ethanol (−100 °C) to purify He gas and Ar gas (only for the sample gas), respectively. In addition, a gas purification tube filled with molecular sieve (1 m) also was used to purify He gas and Ar gas (only for the sample gas). Results showed that there was no significant change in the S background signal in both methods. Therefore, the high purity Ar gas and He gas in this study did not contribute significant S background.

After a series of attempts described above, the sulfur background of ~50% was still remained, which is speculated from entrained air at ICP. It is difficult for us to seal ICP, to achieve a complete isolation of ICP from atmospheric environment. Therefore, the high background of S isotope in LA-MC-ICP-MS is a tricky problem, which seriously affects the sulfur isotope analysis of low-S samples. Compared to LA-MC-ICP-MS, a low background of S is provided by SIMS due to the high vacuum environment in sample cell (~100,000 cps (Hammerli et al., 2021)). Generally, the traditional background correction method is that firstly calculating the average signal intensity in background, and then subtracting it from each sample signal. However, this data correction method ignores the random fluctuation characteristics of background signal itself. When the low-S sample is measured (low S/N), the background signal fluctuation would affect the accuracy of background subtraction by using the average value of background signal. Therefore, we propose using linear regression calculation (LRC) to obtain S isotope ratio for the low-S/N samples.

The LRC was developed for Sr isotope analysis by LA-MC-ICP-MS (Fietzke et al., 2008). It has also been used for the analyses of other isotope ratios in combination with different analytical methods such as gas chromatography MC-ICP-MS (GC-MC-ICP-MS) (Sanabria-Ortega et al., 2012), liquid chromatography MC-ICP-MS (LC-MC-ICP-MS) (Gourgiotis et al., 2017), and capillary electrophoresis MC-ICP-MS (CE-MC-ICP-MS) (Martelat et al., 2018). Fig. 2 shows the traditional method of isotope ratio calculation (point-by-point) and LRC for the same data of S isotope analysis. The slope of the best-fitting straight line represents the $^{34}S/^{32}S$ ratio in Fig. 2b. For LRC method, data does not need background correction. All of data is used to calculate the slope, including the background signal. The advantages of the LRC method will be discussed in detail in section 3.2.

After obtaining the raw $^{34}S/^{32}S$ ratio using both point-by-point method and LRC method, the standard-sample-bracketing (SSB) method was applied to correct instrumental mass bias by repeatedly measuring the standard before and after every five samples. In this study, apatite Sly-1 was used as the matrix-matched external standard due to the homogeneous S isotope composition. The homogeneity verification of Sly-1 is described in section 3.4. The specific S isotope correction formula and calculation formula of δ value referred to Zhang and Hu (2020) and are summarized as follows:

$$\delta^{34}S^{sam}_{V-CDT} = \left(\frac{R_{sample}}{R_{V-CDT}} - 1\right) \times 1000 \tag{1}$$

where R_{sam} and $R_{\mathrm{V\text{-}CDT}}$ are the true isotope ratios in samples and standards, respectively. The accepted standard is Vienna Canyon Diablo Troilite (V-CDT). However, in LA-MC-ICP-MS, international standard material V-CDT is not easily obtained. In addition, the matrix-matched standards were used preferentially to eliminate potential matrix effects. For example, Sly-1 is used as external standard in this study and then the correction equations as follows.

$$\delta^{34}S^{Sly-1}_{V-CDT} = \left(\frac{R_{Sly-1}}{R_{V-CDT}} - 1\right) \times 1000 \tag{2}$$

$R_{\mathrm{Sly\text{-}1}}$ is the true isotope ratios in external standard Sly-1, Eq. 1. is converted to.

$$R_{V-CDT} = \frac{R_{Sly-1}}{\left(\frac{\delta^{34}S^{Sly-1}_{V-CDT}}{1000} + 1\right)} \tag{3}$$

Based on the external calibration:

$$R_{sam} = R_{Sly-1} \times \frac{r_{sam}}{r_{Sly-1}} \tag{4}$$

The r_{sam} and $r_{Sly\text{-}1}$ are the measured isotope ratio in samples and Sly-1, respectively. Then Eq. 3 and 4 can be incorporated into Eq. 1:

$$\delta^{34}S^{sam}_{V-CDT} = \left(\frac{R_{Sly-1} \bullet \frac{r_{sam}}{r_{Sly-1}}}{\frac{R_{Sly-1}}{\left(\frac{\delta^{34}S^{Sly-1}_{V-CDT}}{1000} + 1\right)}} - 1\right) \times 1000 \tag{5}$$

Reducing to the following equation:

$$\delta^{34}S^{sam}_{V-CDT} = \left(\frac{r_{sam}}{r_{Sly-1}} - 1\right) \times 1000 + \frac{r_{sam}}{r_{Sly-1}} \times \delta^{34}S^{Sly-1}_{V-CDT} \tag{6}$$

If r_{sam} is very close to $r_{Sly\text{-}1}$, then $r_{sam}/r_{Sly\text{-}1}$ can be approximated to 1, and the equation is simplified to:

$$\delta^{34}S^{sam}_{V-CDT} \approx \left(\frac{r_{sam}}{r_{Sly-1}} - 1\right) \times 1000 + \delta^{34}S^{Sly-1}_{V-CDT} \tag{7}$$

Equation 7 is widely used in stable isotope analysis of LA-MC-ICP-MS. However, if there is a large difference in the isotopic compositions of the nature samples and Sly-1, the simplified Eq. 7 will cause a wrong value. In this study, $\delta^{34}S_{\mathrm{V\text{-}CDT}}$ value of Sly-1 is 28.41 ± 0.33‰ (2SD), which is a large enough value to result in a potential calculation error. Therefore, we used Eq. 6 to correct the instrumental mass bias and calculate the $\delta^{34}S_{\mathrm{V\text{-}CDT}}$ value of the samples.

The within-run precision for one analysis was 2SE (standard error, k = 2), which be calculated by the combination of 2SE from samples and standards using the following equation:

$$2SE = 2 \times \sqrt{\left(SE_{sample}\right)^2 + \left(SE_{standard-1}\right)^2 + \left(SE_{standard-2}\right)^2} \tag{8}$$

For the traditional correction method (point-by-point), the SE_{sample} is the standard error of the S isotope ratio of sample, $SE_{standard\text{-}1}$ and $SE_{standard\text{-}2}$ are the standard error of the S isotope ratio of the former and the latter bracketing standard, respectively. However, for the LRC method, SE was calculated based on the LINEST function in Microsoft Excel. The relative mathematical formulas have been reported by Feng et al. (2022) at Appendix A. All of the mathematical formulas have been written into an in-house software of "Iso-Compass" (Zhang et al., 2020). Therefore, data processing in this study was completed by using this software to improve work efficiency.

2.2.2. Bulk sulfur isotope analysis using IRMS

Bulk sulfur isotope analysis in apatite was completed at Institute of Geochemistry, Chinese Academy of Sciences, Guiyang, China. Aliquots of the apatite powder were digested a mixture of $NaCO_3$ and ZnO at

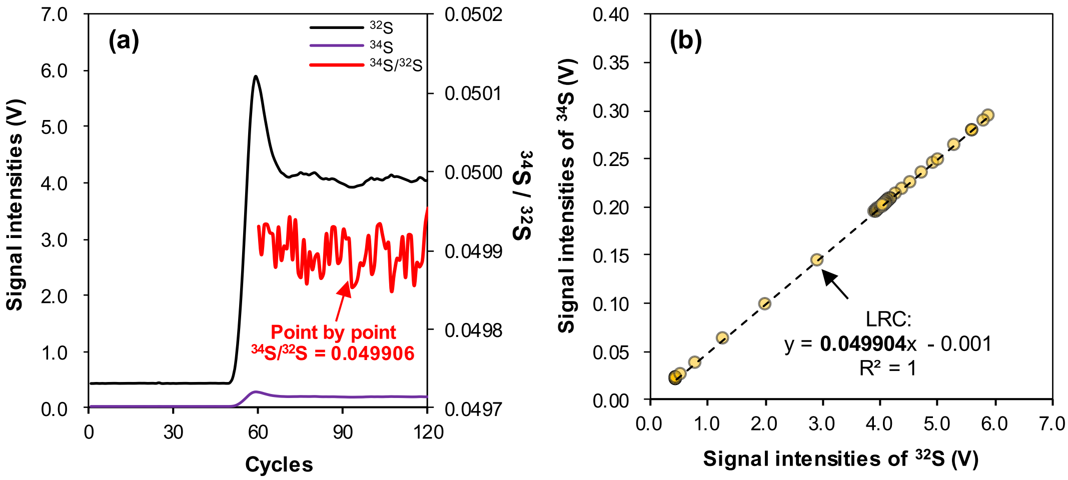

Fig. 2. The typical signal profiles and the raw $^{34}S/^{32}S$ ratios by the traditional point-by-point calculation method when an apatite was analyzed (a). The same data was calculated by LRC method (b).

850 °C for 1 h. Then the reaction product was heated and diluted by ultrapure water to 300 mL, and mixed with $BaCl_2$ solution to precipitate the S in the form of $BaSO_4$. The $BaSO_4$ was then collected by centrifugation and washed to remove leftover acid. The dried $BaSO_4$ was analyzed by elemental analyzer isotope ratio mass spectrometry (EA-IRMS; Flash EA 2000 elemental analyzer, MAT 253, and a Conflo IV continuous flow device produced by Thermo Finnigan). $BaSO_4$ and oxidation catalyst V_2O_5 were added in a tin cup, and then sent into the reactor filled with oxidizing agent WO_3 and reducing agent Cu by automatic sampler. The sample fell into the reaction tube and was sent into oxygen at the same time. At this time, pure oxygen was enriched in the reaction tube, and the sample and tin were rapidly melted and burned to generate SO_2 and SO_3. SO_3 was reduced by Cu to generate SO_2, which was then loaded by helium flow for mass spectrometry. The standard samples used were IAEA-SO-5 (+0.5‰), IAEA-SO-6 (−34.1‰) and NBS 127 (+20.3‰). The analysis results were expressed as $\delta^{34}S$ relative to the international standard V-CDT, and the test accuracy was better than 0.2‰ (1σ).

2.2.3. *Elements determination using electron probe microanalysis (EPMA) and LA-ICP-MS*

The major elements in apatite were obtained by EPMA at Wuhan Sample Solution Analytical Technology Co., Ltd., Wuhan, China, using a JXA-8230 of JEOL instrument equipped with five tunable wavelength-dispersive spectrometers. The minerals were analyzed under an accelerating voltage of 15 kV and a probe current of 20 nA. The beam spot diameter was 3 μm and the average detection limits for each element were 0.01%. The analyzed elements include Ca, K, Ti, Na, Mg, Al, Mn, Fe, Sr, SO_3, P, Si, F, Cl were measured. The analytical results were listed in Table S1. The calibration standard samples for the content of major elements use 53 kinds of mineral standard samples, 44 kinds of elemental standard samples and 15 kinds of rare earth element standard samples provided by SPI company. The data correction method adopts the ZAF correction method of JEOL. Based on the measured major elements and other published apatite data from GEOROC database, we can find that most apatites in this study are F-rich apatite (Fig. 3a).

Trace element compositions in apatite were measured at the State Key Laboratory of Geological Processes and Mineral Resources (GPMR Lab), China University of Geosciences (Wuhan), following the method of Liu et al. (2008). An Agilent 7900 quadrupole ICP-MS combined with a GeoLas Pro 193 nm excimer laser platforms were used. Ablation was conducted in a helium atmosphere after which argon gas added immediately after the cell to aid transport of material. The laser ablation parameters were set at a spot size of 44 μm, a repetition rate of 5 Hz and a fluence of ~4–5 J cm^{-2}. NIST 610 was used to optimum sensitivity while keeping the ThO^+/Th^+ ratio below 0.5% and the U^+/Th^+ ratio close to 1. Each LA-ICP-MS analysis incorporated an approximately 20 s background acquisition followed by 50 s of data acquisition from the sample. NIST SRM 610 was repetitively analyzed every ten sample analyses for time-drift correction. BCR-2G, BHVO-2G and BIR-1G were used as external standards. *ICPMSDataCal* software edited by Liu et al. (2008) was used to perform the offline selection and integration of background and ablation signals, time-drift correction and quantitative calibration.

All data of major elements and trace elements in apatite using EPMA and LA-ICP-MS are listed in Table S2 and Table S3.

3. Results and discussion

3.1. *Effect of laser ablation parameters on S isotope ratios*

Previous studies have found strong fractionation of S isotopes in sulfides during ablation (Bendall et al., 2006; Craddock et al., 2008; Gilbert et al., 2014; Zhu et al., 2017). Gilbert et al. (2014) reported a large fractionation effect for ablating pyrite with the New Wave Nd:YAG 193 nm laser. Zhu et al. (2017) showed a fractionation up to 2‰ of $\delta^{34}S$ during analysis of pyrite with different laser parameters using a 193 nm ArF excimer laser. Fu et al. (2017) investigated the effect of 257 nm femtosecond (fs) and 193 nm ArF excimer nanosecond (ns) laser ablation systems on S isotope analysis. The authors demonstrated the fs-laser system has less fluence, therefore avoiding partial melting, and matrix dependent S isotopic fractionation. In this study, fs-LA system was also applied to eliminate or attenuate potential S isotope fractionation behavior during the laser ablation processing. A natural apatite Sly-1 was analyzed with different laser ablation parameters, including laser fluence, spot size, laser pulse rate.

Firstly, the $\delta^{34}S$ values were measured under nine different laser fluence values (from 0.3 to 3.0 J cm^{-2}) with a given laser spot size of 60 μm, ablation frequency of 50 Hz and line scan rate of 5 μm s^{-1}. Data presented are relative to the laser fluence of 1.2 J cm^{-2}. Results show that the S/N value continued to grow with the laser fluence increase from 0.3 to 2.3 J cm^{-2}, and was stable when fluence increased from 2.3 to 3 J cm^{-2} (Fig. 4a). But there was no fluence dependent fractionation for the S isotope ratios over the whole range of fluence values. At the laser fluence of 0.3 and 0.5 J cm^{-2}, the low S/N values were obtained (0.6 and 2.5, respectively), causing large analytical precisions of $\delta^{34}S$. Next, the $\delta^{34}S$ values were determined at various spot size from 10 μm to 60 μm with a given laser fluence of 2.1 J cm^{-2}, ablation frequency of 50 Hz and line scan rate of 5 μm s^{-1}. All data were normalized to the result of 60 μm. Results follow the same trend of the laser fluence test. No obvious variation of $\delta^{34}S$ was observed, and S/N values are positively correlated with spot sizes (Fig. 4b). A large analytical precision of $\delta^{34}S$

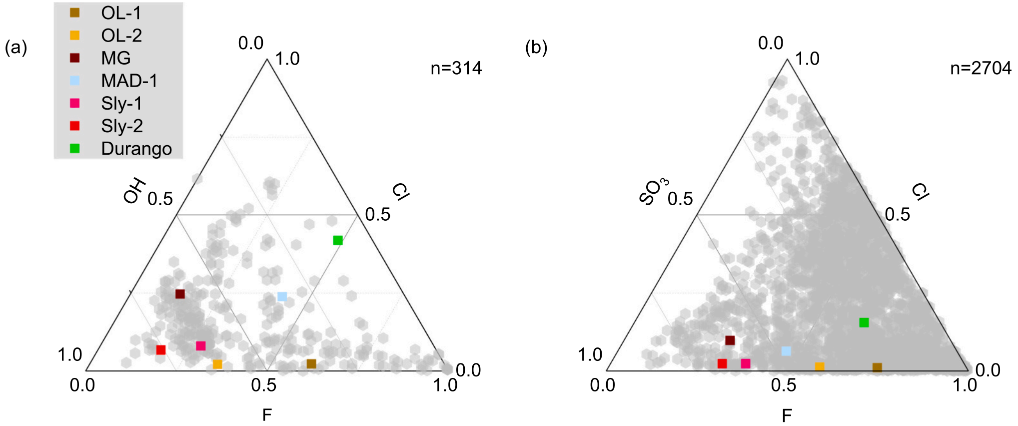

Fig. 3. Ternary plots showing halogen, OH and SO_3 contents of apatites analyzed in this study. Concentrations of F, Cl and SO_3 were measured by EPMA with OH being predicted from charge balance assuming the halogen site is full. In addition, other published F-Cl-OH-SO_3 data in apatites are listed for comparision, which were obtained from the GEOROC Compilation database (GRO.data: https://data.goettingen-research-online.de/dataverse/gro).

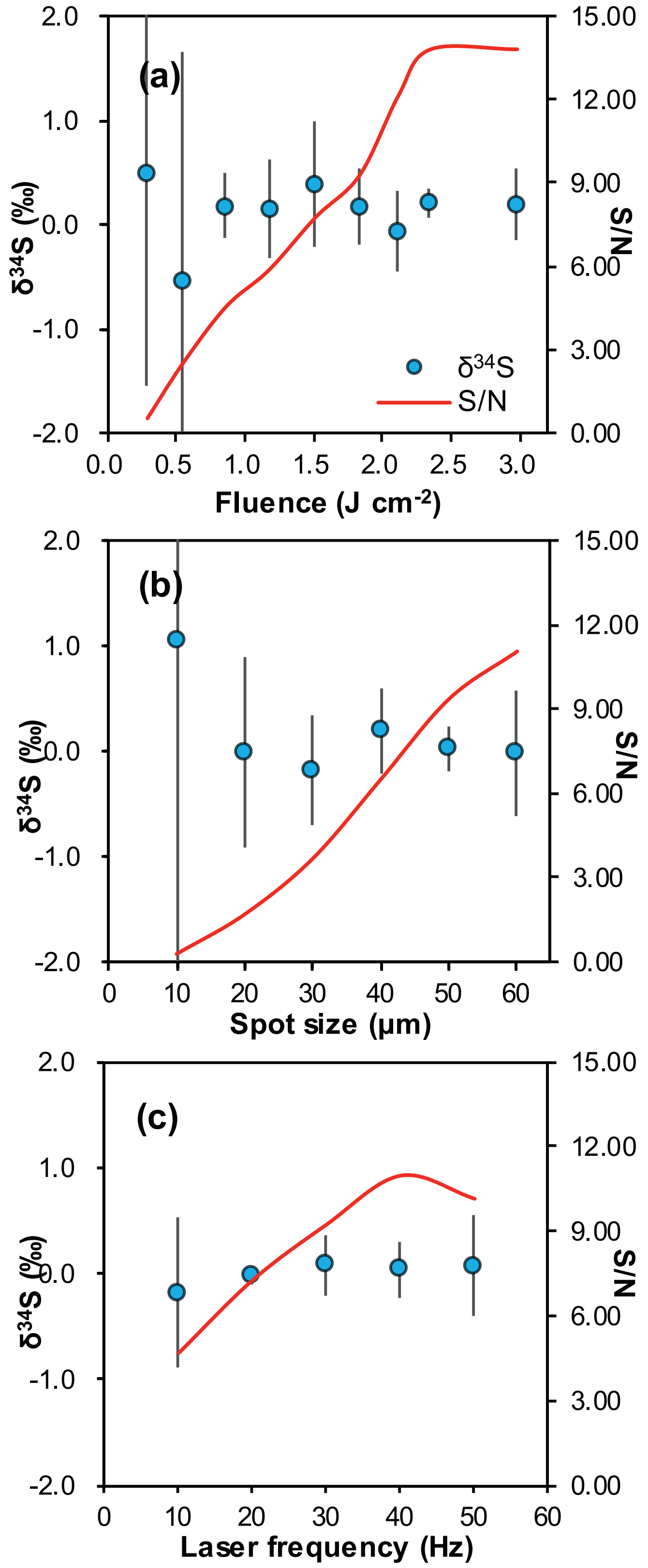

Fig. 4. Investigating the variation of $\delta^{34}S$ and S/N ratio as function of the laser fluence (a), spot size (b), laser frequency (c) through repeatedly measuring Sly-1. The blue dots represent $\delta^{34}S$ values with error bars of 2SD, and the red lines represent the S/N ratios.

was obtained when spot size of 10 μm was applied and S/N was reduced to 0.3. At last, we investigated the effect of laser frequency from 10 Hz to 50 Hz with a given laser fluence of 2.1 J cm^{-2}, spot size of 60 μm and line scan rate of 5 μm s^{-1}. All data were normalized to the result of 50 Hz. The S/N value continued to grow with the laser frequency from 10 to 40 Hz, and was stable or slightly decrease when the laser frequency was higher than 40 Hz (Fig. 4c). There was no laser frequency dependent fractionation for the S isotope ratios.

The results showed that the routine parameters of fs laser system did not influence the measurement of S isotope ratio in apatite. Some slight variations in $\delta^{34}S$ were observed and attributed to the low S/N ratio. When S/N ratios are higher than 5.0, a good reproducibility of $\delta^{34}S$ (<0.5‰) at different laser parameters can be obtained. The typical surface morphology of laser ablation crater and deposited aerosol particles are characterized by SEM and showed in Fig. 5. The irregular and rough ablation crater were formed due to the Gaussian energy beam profile of fs laser system. Moreover, few melting rims were observed around the laser crater, indicating that the thermal process of apatite ablation in the fs laser was suppressed. Fu et al. (2017) has reported that fs-laser can provide the less fluence and matrix dependent S isotopic fractionation, smaller size of particles and less thermal effect during the sulfide ablation, compared to nanosecond (ns) laser system. Therefore, we speculate that the stable $\delta^{34}S$ values at different laser parameters were caused by the advantage of fs laser of low thermal effect during the apatite ablation process. This is an important advantage for the natural apatite analysis, because the laser ablation parameters (spot size and ablation frequency) should be changed during the measurement of natural apatites with various size, complex structure or growth zoning.

3.2. *The effect of data reduction processes on the analytical precision in low-sulfide apatite samples*

As discussed in section 3.1., the high signal of S isotopes in the background affects the determination of $\delta^{34}S$ in low-S apatite samples (low S/N ratio). In order to resolve this problem, a new LRC method was attempt to instead of the traditional data reduction method to calculate the raw $^{34}S/^{32}S$ ratio. We used same parameters in laser system and MC-ICP-MS to analyze seven natural apatites in an individual experimental session and then calculate the raw $^{34}S/^{32}S$ ratios, within-run precision and intermediate precision using the traditional point-by-point method and LRC method. Note that the within-run precision represents the precision of an individual analysis and was expressed as two times standard error (2SE), the intermediate precision represents the analytical reproducibility in one apatite sample and was expressed as the two times standard deviation (2SD). Moreover, we calculated the theoretical precision of $^{34}S/^{32}S$ ($2SD_p$) based on the signal intensities of ^{34}S and ^{32}S and a computational formula from Yang et al. (2011). Fig. 6a shows the within-run precision (2SE) from both data reduction methods as a function of the intensity of ^{32}S and the ratio of S/N. An obvious negative correlation between ^{32}S signal intensities (and S/N ratios) and within-run precisions is observed in both data reduction processes (Fig. 6a). Sly-1, Sly-2, MAD-1 and MG have high concentrations of SO_3 from 0.93 to 1.26, and hence obtained high signal of ^{32}S from 1.40 to 3.18 V and high S/N ratios from 4.7 to 10.6. The point-by-point method and LRC method both provided good within-run precisions, which were close to the theoretical precisions ($2SD_p$) (Fig. 6a). However, when the low-S samples of Durango (SO_3 = 0.41%), OL-1 (SO_3 = 0.21%) and OL-2 (SO_3 = 0.34%) were analyzed, the ^{32}S signal and S/N decreased to 0.32 V ~ 1.10 V and 1.0–3.7, respectively. Both methods show the higher within-run precisions than theoretical precisions ($2SD_p$). But the within-run precision calculated by LRC method were lower than those by point-by-point method (Fig. 6a), indicating the better performance of LRC method for the low S/N ratio data.

The intermediate precisions (2SD) are controlled by the presented method, signal intensity of the isotopes and the homogeneity of S isotopic compositions in samples. Therefore, a difference between the

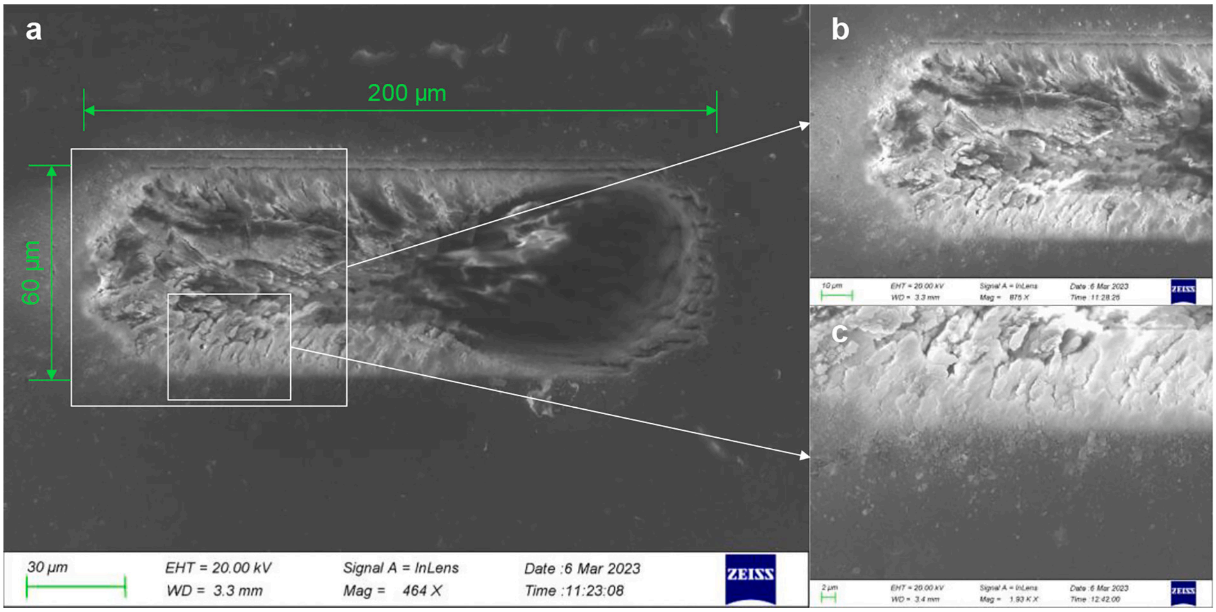

Fig. 5. SEM images of the laser ablation crater in Sly-1 produced with spot size of 60 µm, laser frequency of 50 Hz, speed rate of 5 µm s^{-1}, and laser fluence of 2.11 J cm^{-2}.

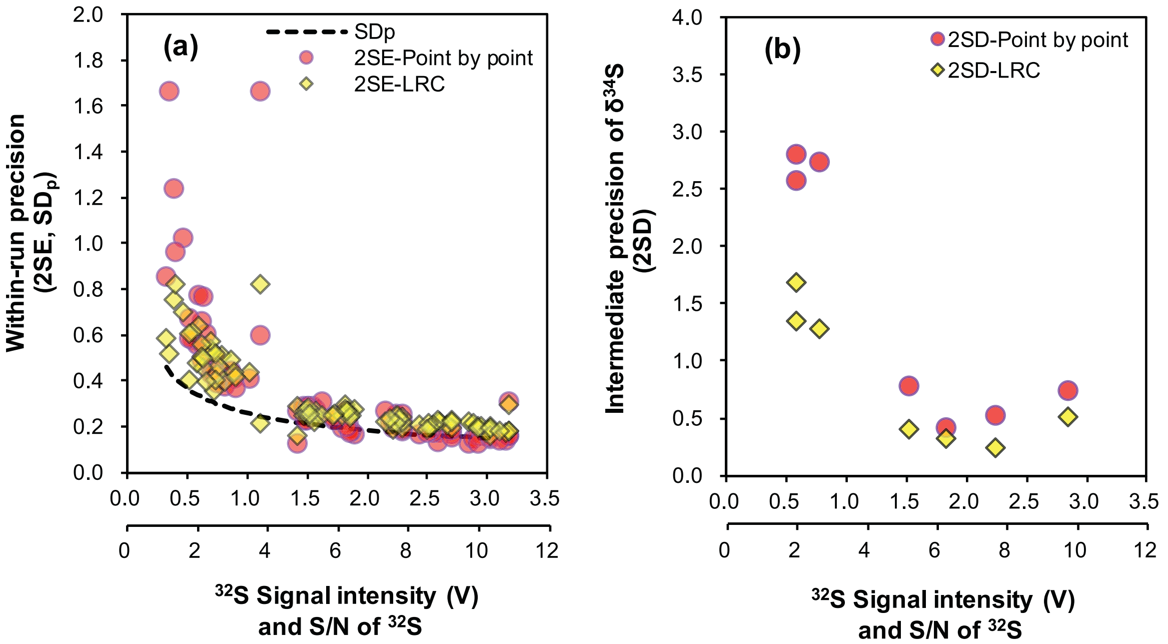

Fig. 6. The relationship between S signal intensities (and S/N ratios) and within-run precision (a) and intermediate precision (b). The same data were calculated using point-by-point method and LRC method. A theoretical precision of SDp based on the signal intensities of ^{34}S and ^{32}S and a computational formula from Yang et al. (2011) is shown in plot (a).

intensities of ^{32}S and intermediate precisions was observed, such as that Sly-2 shows the highest ^{32}S signal and S/N ratio but has a slightly high intermediate precision (Fig. 6b). Nonetheless, we also can summarize some rough regularities from the data. A negative correlation between ^{32}S signal intensities (and S/N ratios) and intermediate precisions is found in both data reduction processes. All of the data indicate that LRC method provide better intermediate precisions than point-by-point method, and this advantage is even more pronounced at low signals and low S/N ratios (Fig. 6b).

In summary, LRC method can process the S isotope data with better performance, especially for the low signals of ^{32}S (<1 V) or low S/N ratios (<~3). For the high-S apatites, the combination of the presented instrument parameters and LRC method would provide the within-run precisions and intermediate precisions from 0.16‰ to 0.30‰ and from 0.24‰ to 0.51‰, respectively. However, when the concentrations of SO_3 as low as 0.2%–0.4%, the within-run precisions and intermediate precisions would worsen, and from 0.41‰ to 0.82‰ and from 1.28‰ to 1.68‰, respectively. Please note that both within-run precision and intermediate precision are greatly affected by the sensitivity of MC-ICP-MS. Therefore, if the sensitivity of MC-ICP-MS becomes better or worse in different experimental periods, the within-run precision and intermediate precision could be a corresponding improvement or deterioration.

3.3. *Accurate determination $\delta^{34}S_{V\text{-}CDT}$ in apatite using fs-LA-MC-ICP-MS*

The $\delta^{34}S_{V\text{-}CDT}$ values in seven natural apatites were analyzed by fs-LA-MC-IC-MS over six months with different sessions. Optimized laser ablation parameters were used with the laser spot size of 50 μm, laser frequency of 50 Hz, laser fluence of ~3 J cm^{-2} and line scan mode (5 μm s^{-1}). We tried to use pyrite as an external calibration standard to correct the mass fractionation of apatite. But a lager analytical error was obtained (~2.0‰), indicating there is a matrix effect between pyrite and apatite during LA-MC-ICP-MS analysis. Therefore, the apatite Sly-1 was used as the matrix-matched external standard in this study. The summarized data, including the $\delta^{34}S_{V\text{-}CDT}$ values obtained by bulk-sample analyses and LA-MC-ICP-MS analyses, the concentrations of SO_3 and other apatites data from previous studies, are listed in Table 3, Table S4 and Fig. 7.

Sly-1, Sly-2 and MG have high concentrations of SO_3, from 1.17% to 1.26%. These results from LA-MC-ICP-MS agree with those from IR-MS with a good intermediate precision (0.46‰-0.62‰). OL-1 and OL-2 have very low concentrations of SO_3 (0.21% and 0.34%, respectively). The measured results of $\delta^{34}S_{V\text{-}CDT}$ in OL-1 and OL-2 are consistent with the IR-MS values, but showed a large intermedia precision (0.88‰-1.16‰). MAD-1 was collected from Madagascar and has been used as reference materials for Sr isotope analysis in many micro-labs (Yang et al., 2014; Kennedy et al., 2023). The measured $\delta^{34}S_{V\text{-}CDT}$ values from IR-MS and LA-MC-ICP-MS were 12.92 ± 0.05‰ and 13.55 ± 0.58‰ (2SD), respectively. A slightly large discrepancy of >0.63 ‰ between IR-MS and LA-MC-ICP-MS was observed. Kennedy et al. (2023) also reported the $\delta^{34}S_{V\text{-}CDT}$ values of MAD, which were 13.30‰ and 12.70 ± 0.88‰ (2SD) obtained from IR-MS and SIMS, respectively. Our results of MAD from LA-MC-ICP-MS were closer to the IR-MS value from Kennedy et al. (2023). We speculate that the MAD apatite used for bulk analyses in this study had a slightly different S isotope composition than the material analyzed by LA-MC-ICP-MS, and MAD also could have heterogeneous S isotope compositions in different fragments. The apatite Durango is a widely used apatite reference material. Previous studies have reported $\delta^{34}S_{V\text{-}CDT}$ values of Durango using different methods, including 0.34 ± 0.04‰ (Economos et al., 2017), −1.06 ± 0.80‰ (Hammerli et al., 2021) and − 1.39 ± 0.48‰ (Hammerli et al., 2021) through bulk analyses, and 0.33 ± 0.63‰ (Hammerli et al., 2021), −1.57 ± 0.85‰ and − 1.60 ± 1.24‰ (Hammerli et al., 2021), −3.30 ± 0.92‰ (Kennedy et al., 2023) through SIMS. In this study, we reported the $\delta^{34}S_{V\text{-}CDT}$ values of Durango of −1.24 ± 1.09‰, which falls within the range of previous reported values and provides a comparable intermediate precision.

The micro-analysis of $\delta^{34}S_{V\text{-}CDT}$ in apatite was first developed by SIMS (Economos et al., 2017). Hammerli et al. (2021) then reported and discussed the precision, accuracy, matrix effect, and crystal orientation effect on $\delta^{34}S_{V\text{-}CDT}$ analysis using SIMS in detail. The previous studies have determined the $\delta^{34}S_{V\text{-}CDT}$ values in more than fifteen natural apatites using SIMS. In this study, we presented the first micro-method to analyze $\delta^{34}S_{V\text{-}CDT}$ in apatite using LA-MC-ICP-MS. Fig. 7a shows the relationship between the measured results from SIMS and this study (LA-MC-ICP-MS) to the bulk method. Results confirmed that an accurate $\delta^{34}S_{V\text{-}CDT}$ determination in apatite can be obtained using LA-MC-ICP-MS. Moreover, a similar intermedia precision (2SD) between LA-MC-ICP-MS and SIMS can be achieved when the concentration of SO_3 is >0.3 (wt%) (Fig. 7b). In addition, previous results have confirmed that SIMS sulfur isotope measurements have not identified chemical matrix or crystallographic orientation effects (Hammerli et al., 2021). However, the primary beam of SIMS seems to influence the S isotope measurement, for example the $\delta^{34}S_{V\text{-}CDT}$ values of 11.29 ± 0.62‰, 12.65 ± 0.48‰, 13.23 ± 0.38‰ in GR40 apatite were obtained by 1 nA, 2 nA, and 3 nA, respectively (Kennedy et al., 2023). This phenomenon indicates that a rigorous optimization of instrument conditions in SIMS is required. However, LA-MC-ICP-MS showed a stable $\delta^{34}S_{V\text{-}CDT}$ values at different laser ablation parameters in this study (Fig. 4), confirming a more tolerant and robust analytical performance.

The major shortcomings of LA-MC-ICP-MS are bad spatial resolution. The typical laser ablation crater in this study is a line with diameter of

Table 3
Data summary of S concentrations and isotopic compositions from bulk analysis and mirco-analysis in published articles and this study.

Sample name	SO_3 (wt%)	2SD	Bulk analysis		Methods	$\delta^{34}S_{V\text{-}CDT}$(‰)	2SD	Methods	References
			$\delta^{34}S_{V\text{-}CDT}$(‰)	2SD					
Durango	0.36	0.04	0.34	0.04	GS-MS	0.33	0.63	SIMS	Economos, et al., (2017)
SAP1	0.55	0.06	12.27[a]	0.22	Fluorination, MC-ICP-MS, IR-MS	12.52	0.89	SIMS	Hammerli, et al., (2021)
SAP2	0.78	0.08	12.46[a]	0.22	Fluorination, MC-ICP-MS, IR-MS	13.79	0.53	SIMS	Hammerli, et al., (2021)
SAP3	0.59	0.06	12.85[a]	0.60	Fluorination, MC-ICP-MS, IR-MS	13.54	0.97	SIMS	Hammerli, et al., (2021)
Big1	0.75	0.04	14.02[a]	0.22	Fluorination, MC-ICP-MS, IR-MS	13.58	0.70	SIMS	Hammerli, et al., (2021)
Hormuz	0.07	0.02	25.78[a]	0.60	Fluorination, MC-ICP-MS, IR-MS	25.48	3.37	SIMS	Hammerli, et al., (2021)
Mdg-1	0.04	0.02	1.42[a]	0.60	Fluorination, MC-ICP-MS, IR-MS	−0.50	2.46	SIMS	Hammerli, et al., (2021)
Durango-A	0.31	0.10	−1.06[a]	0.80	Fluorination, MC-ICP-MS, IR-MS	−1.57	0.85	SIMS	Hammerli, et al., (2021)
Durango-B	0.29	0.04	−1.39[a]	0.48	Fluorination, MC-ICP-MS, IR-MS	−1.60	1.24	SIMS	Hammerli, et al., (2021)
OL2	0.51	0.05	9.15	–	IR-MS	8.75	0.66	SIMS	Kennedy, et al., (2023)[b]
OL4	0.23	0.01	11.16	–	IR-MS	7.84	0.52	SIMS	Kennedy, et al., (2023)[b]
GR40	0.67	0.04	14.69	–	IR-MS	13.23	0.38	SIMS	Kennedy, et al., (2023)[b]
AFB 1	1.12	0.01	13.69	–	IR-MS	15.00	1.10	SIMS	Kennedy, et al., (2023)[b]
SLAP	0.87	0.02	13.39	–	IR-MS	13.39	0.30	SIMS	Kennedy, et al., (2023)[b]
MADAP	0.69	0.03	13.30	–	IR-MS	12.70	0.88	SIMS	Kennedy, et al., (2023)[b]
BR96	0.87	0.03	19.01	–	IR-MS	19.72	0.58	SIMS	Kennedy, et al., (2023)[b]
AFG2	1.23	0.05	17.04	–	IR-MS	18.46	0.42	SIMS	Kennedy, et al., (2023)[b]
Durango-B	0.29	0.04				−3.30	0.92	SIMS	Kennedy, et al., (2023)[b]
Sly-1	1.21	0.42	28.41	0.33	IR-MS	28.39	0.46	LA-MC-ICP-MS	This study
Sly-2	1.26	0.07	28.78	0.63	IR-MS	28.72	0.56	LA-MC-ICP-MS	This study
MAD-1	0.93	0.18	12.92	0.04	IR-MS	13.55	0.58	LA-MC-ICP-MS	This study
MG	1.17	0.04	13.51	0.57	IR-MS	13.04	0.62	LA-MC-ICP-MS	This study
OL-1	0.21	0.30	10.06	0.12	IR-MS	9.53	0.88	LA-MC-ICP-MS	This study
OL-2	0.34	0.33	10.15	0.18	IR-MS	10.42	1.16	LA-MC-ICP-MS	This study
Durango	0.41	0.20	–	–	–	−1.24	1.09	LA-MC-ICP-MS	This study

[a] A average value of $\delta^{34}S_{V\text{-}CDT}$(‰) from three different bulk analysis method, including fluorination method, MC-ICP-MS and IR-MS.

[b] The $\delta^{34}S_{V\text{-}CDT}$(‰) data from Kennedy et al. (2023) are collceted from session 5 with a 3 nA primary beem of SIMS.

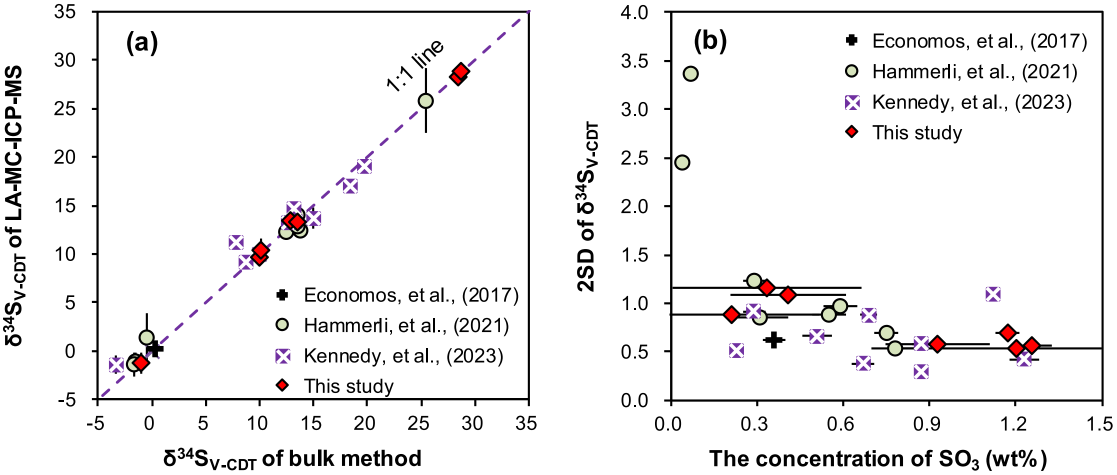

Fig. 7. A comparison of $\delta^{34}S_{V\text{-}CDT}$ (‰) using bulk analysis and micro-analysis in this study (a) and a relationship between the concentrations of SO_3 (wt%) and intermediate precisions of $\delta^{34}S_{V\text{-}CDT}$ (2SD) (b). The published data from SIMS (Economos et al., 2017; Hammerli et al., 2021; Kennedy et al., 2023) are also shown in both plots.

60 μm and length of 200 μm (Fig. 5), which is larger than that of SIMS (spot size of 10–20 μm). Additionally, the precision of low-S apatites ($SO_3 < 0.3$ wt%) would be worse than 1.5‰, which is not enough to recognize the natural variations in S isotopic ratios. Both problems are mainly attributed to the high background of S isotopes in MC-ICP-MS. Therefore, reducing the background signal of S isotopes is an important factor to improving the spatial resolution and analytical precision for the low-S apatites. Unfortunately, this study did not address the problem of high background. Moreover, we cannot analyze $\delta^{33}S_{V\text{-}CDT}$ due to the low signal of ^{33}S. So, our method cannot provide the multiple S isotope information like SIMS.

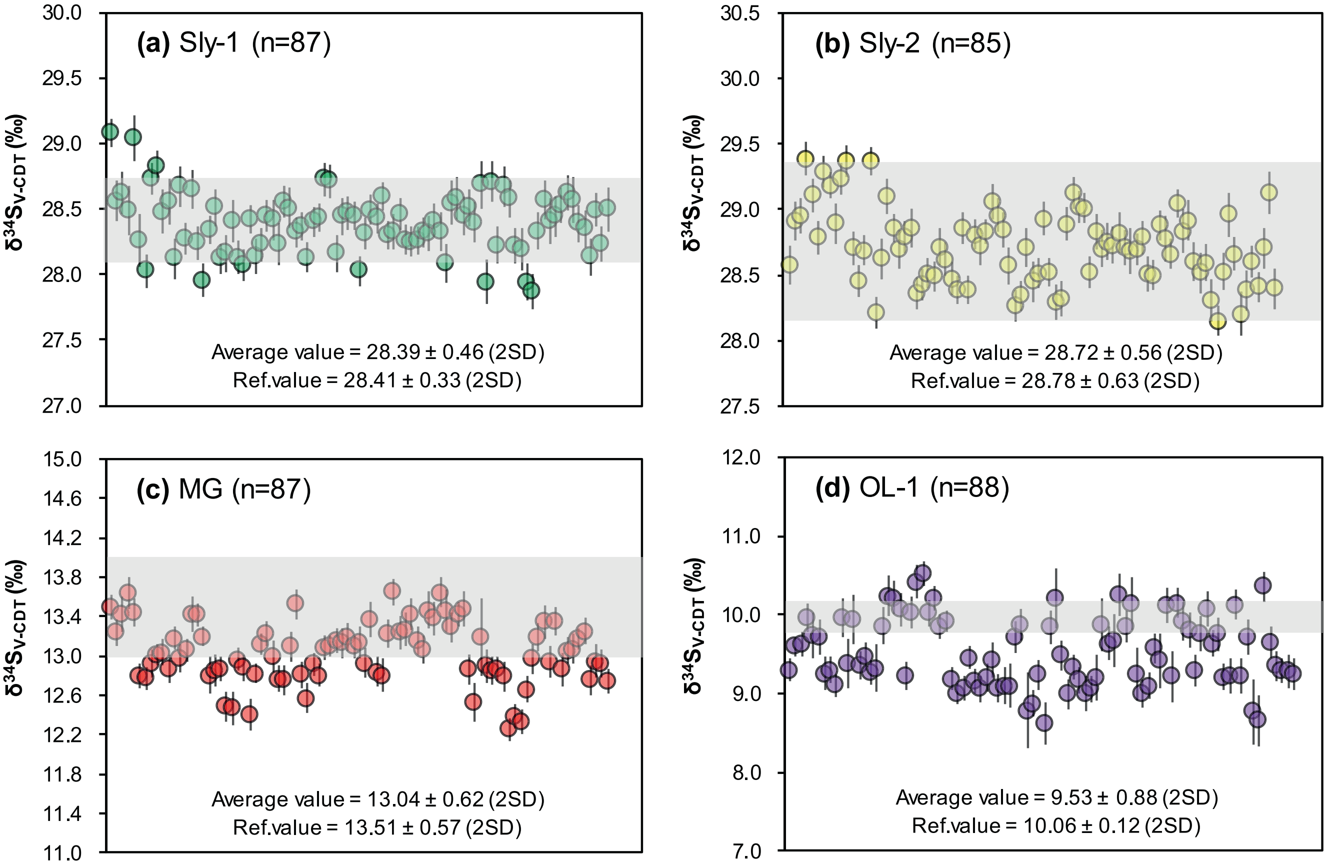

Fig. 8. A compilation of $\delta^{34}S_{V\text{-}CDT}$ (‰) in four apatites (Sly-1, Sly-2, MG, and OL-1) obtained from repeated measurements in different analytical sessions. Error bars represent the with-run precision. The reference values from bulk analysis are plotted as the grey area.

3.4. The potential reference materials of apatites for S isotope analysis (Sly-1, Sly-2, MG, and OL-1)

The $\delta^{34}S_{V\text{-}CDT}$ values of Sly-1, Sly-2, MG, and OL-1 in Table S4 were obtained from the repeatedly analysis of different fragments. More than thirty fragments of each apatite (1–2 mm size) were selected randomly, and S isotopes were measured at different experimental sessions. A good homogeneity of S isotope compositions in four apatites (Sly-1, Sly-2, MG, and OL-1) is observed (Table S4 and Fig. 8). Note that a difference of $\delta^{34}S_{V\text{-}CDT}$ between IR-MS and LA-MC-ICP-MS in MG and OL-1 is observed (−0.47‰ and − 0.53‰, respectively, Fig. 8c and d). This is mainly attributed to the selection of samples. IR-MS method should consume about 0.3–0.5 g samples for one measurement. The cracks and inclusions in the samples may affect the results of sulfur isotope analysis by IR-MS. However, these potential interference factors can be avoided in LA-MC-ICP-MS. In addition, the analytical precision of $\delta^{34}S_{V\text{-}CDT}$ in apatites is poorer than that in S-rich sulfide minerals. Therefore, analytical results could slightly deviate from the IR-MS results due to its poor analytical precision, especially OL-1. However, considering that the sulfur content of OL-1 is only 0.21% and the generally analytical precision for these low-S apatites is ~1‰ in SIMS and LA-MC-ICP-MS, we suggest that the current analytical deviation between IR-MS and LA-MC-ICP-MS is acceptable. Sly-1, Sly-2 and MG, which have high concentrations of SO_3 from 1.17% to 1.21%, showed similar intermediate precisions from 0.46‰ to 0.62‰. The concentration of SO_3 in OL-1 is low and similar to Durango apatite (0.29%–0.36%, Table 3). A large deviation of $\delta^{34}S_{V\text{-}CDT}$ in Durango has been found, such as $\delta^{34}S_{V\text{-}CDT}$ = 0.33 ± 0.63‰ from Economos et al. (2017), = −1.57 ± 0.85‰ and −1.60 ± 1.24‰ from Hammerli et al. (2021), = −3.30 ± 0.92‰ from Kennedy et al. (2023). But OL-1 shows a more homogenous S isotope composition (2SD = 0.88‰), indicating a greater potential as a reference material for the low-S apatite analysis. We think that the four apatites have the potential as the external standards for *in situ* S isotope analysis for LA-MC-ICP-MS and SIMS. In addition, the ideal natural reference materials should be available in sufficient quantities as to be usable by the broader geological community, especially for LA-MC-ICP-MS due to the high consumption. In this study, the amount of Sly-1 (5.68 g), Sly-2 (14.50 g), MG (44.79 g) and OL-1 (13.74 g) is sufficient for distribution to a large number of labs around the world. Note that the average amount of proposed apatites from Kennedy et al. (2023) only 0.3–1.5 g in eleven apatites, except BR96 with a large weight of 18 g. But the large $\delta^{34}S_{V\text{-}CDT}$ values in BR96 from 17.77‰ to 19.72‰ indicate the heterogeneity of S isotope composition in BR96.

4. Conclusion

This study presents a precise and accurate S isotopic analysis method using fs-LA-MC-ICP-MS in apatite. The high background of S in MC-ICP-MS and the low-concentration of S in apatite both seriously impede the S isotope analysis in LA-MC-ICP-MS. A detailed investigation found that half the S background can be removed by cleaning or replacing the transformation system of aerosol particles, but other half could be entrained air at ICP and hardly resolved by the current commercial instruments. A new calculation method of LRC was proposed to process the S isotope ratio and improved the analytical precision for the low-S/N samples obviously. Fs laser system was used to reduce the potential S isotope fractionation induced by laser ablation process. The analytical results of seven natural apatites by fs-LA-MC-ICP-MS are excellent agreement with the bulk analysis values, while the intermedia precision in the presented method is comparable with that from SIMS. Moreover, four apatites (Sly-1, Sly-2, MG, and OL-1) with various concentrations of SO_3 and large quantities show the homogeneous S isotope compositions, suggesting they can serve as external reference materials for *in situ* S isotope analysis for LA-MC-ICP-MS and SIMS.

Declaration of Competing Interest

The authors declare that they have no known competing financial interests or personal relationships that could have appeared to influence the work reported in this paper.

Data availability

The data is included in the supporting information.

Acknowledgements

This research is supported by the National Key Research and Development Program of China (2021YFC2903003), the National Natural Science Foundation of China (Grants 41973013), the most special fund from the State Key Laboratories of Geological Processes and Mineral Resources, China University of Geosciences (MSFGPMR04 and MSFGPMR08).

Appendix A. Supplementary data

Supplementary data to this article can be found online at https://doi.org/10.1016/j.chemgeo.2023.121651.

References

Belousova, E.A., Griffin, W.L., O'Reilly, S.Y., Fisher, N.I., 2002. Apatite as an indicator mineral for mineral exploration: trace-element compositions and their relationship to host rock type. J. Geochem. Explor. 76 (1), 45–69.

Bendall, C., Lahaye, Y., Fiebig, J., Weyer, S., Brey, G.P., 2006. *In situ* sulfur isotope analysis by laser ablation MC-ICPMS. Appl. Geochem. 21 (5), 782–787.

Brounce, M., Boyce, J., McCubbin, F.M., Humphreys, J., Reppart, J., Stolper, E., Eiler, J., 2019. The oxidation state of sulfur in lunar apatite. Am. Mineral. 104 (2), 307–312.

Chew, D.M., Spikings, R.A., 2021. Apatite U—Pb thermochronology: a review. Minerals 11 (10), 1095.

Craddock, P.R., Rouxel, O.J., Ball, L.A., Bach, W., 2008. Sulfur isotope measurement of sulfate and sulfide by high-resolution MC-ICP-MS. Chem. Geol. 253 (3–4), 102–113.

Dempster, T.J., Jolivet, M., Tubrett, M.N., Braithwaite, C.J.R., 2003. Magmatic zoning in apatite: a monitor of porosity and permeability change in granites. Contrib. Mineral. Petrol. 145 (5), 568–577.

Doherty, A.L., Webster, J.D., Goldoff, B.A., Piccoli, P.M., 2014. Partitioning behavior of chlorine and fluorine in felsic melt-fluid(s)-apatite systems at 50 MPa and 850–950 °C. Chem. Geol. 384, 94–111.

Economos, R., Boehnke, P., Burgisser, A., 2017. Sulfur isotopic zoning in apatite crystals: A new record of dynamic sulfur behavior in magmas. Geochim. Cosmochim. Acta 215, 387–403.

Feng, Y., Zhang, W., Hu, Z., Liu, Y., Luo, T., He, T., Liu, H., Yu, K., 2022. A new analytical mode and application of the laser ablation inductively coupled plasma mass spectrometer in the earth sciences. Sci. China Earth Sci. 65 (1), 182–196.

Fietzke, J., Liebetrau, V., Guenther, D., Guers, K., Hametner, K., Zumholz, K., Hansteen, T.H., Eisenhauer, A., 2008. An alternative data acquisition and evaluation strategy for improved isotope ratio precision using LA-MC-ICP-MS applied to stable and radiogenic strontium isotopes in carbonates. J. Anal. At. Spectrom. 23 (7), 955–961.

Fu, J., Hu, Z., Zhang, W., Yang, L., Liu, Y., Li, M., Zong, K., Gao, S., Hu, S., 2016. *In situ* sulfur isotopes ($\delta^{34}S$ and $\delta^{33}S$) analyses in sulfides and elemental sulfur using high sensitivity cones combined with the addition of nitrogen by laser ablation MC-ICP-MS. Anal. Chim. Acta 911, 14–26.

Fu, J., Hu, Z., Li, J., Yang, L., Zhang, W., Liu, Y., Li, Q., Zong, K., Hu, S., 2017. Accurate determination of sulfur isotopes ($\delta^{33}S$ and $\delta^{34}S$) in sulfides and elemental sulfur by femtosecond laser ablation MC-ICP-MS with non-matrix matched calibration. J. Anal. At. Spectrom. 32 (12), 2341–2351.

Gilbert, S.E., Danyushevsky, L.V., Rodemann, T., Shimizu, N., Gurenko, A., Meffre, S., Thomas, H., Large, R.R., Death, D., 2014. Optimisation of laser parameters for the analysis of sulfur isotopes in sulphide minerals by laser ablation ICP-MS. J. Anal. At. Spectrom. 29 (6), 1042–1051.

Gourgiotis, A., Manhès, G., Martelat, B., Isnard, H., 2017. Deconvolution of the isotopic drift in LC-MC-ICPMS coupling: a new tool for studying isotope fractionation induced by sample introduction techniques. J. Anal. At. Spectrom. 32 (7), 1428–1434.

Hammerli, J., Greber, N.D., Martin, L., Bouvier, A., Kemp, A.I.S., Fiorentini, M.L., Spangenberg, J.E., Ueno, Y., Schaltegger, U., 2021. Tracing sulfur sources in the crust *via* SIMS measurements of sulfur isotopes in apatite. Chem. Geol. 579, 120242.

Hasebe, N., Barbarand, J., Jarvis, K., Carter, A., Hurford, A.J., 2004. Apatite fission-track chronometry using laser ablation ICP-MS. Chem. Geol. 207 (3–4), 135–145.

Jennings, E.S., Marschall, H.R., Hawkesworth, C.J., Storey, C.D., 2011. Characterization of magma from inclusions in zircon: apatite and biotite work well, feldspar less so. GEOLOGY 39 (9), 863–866.

Kennedy, A.K., Wotzlaw, J.F., Crowley, J.L., Schmitz, M., Schaltegger, U., Wade, B., Martin, L., Talavera, C., Ware, B., Bui, T.H., 2023. Apatite reference materials for SIMS microanalysis of isotopes and trace elements. Geostand. Geoanal. Res. 47, 373–402.

Konecke, B.A., Fiege, A., Simon, A.C., Parat, F., Stechern, A., 2017. Co-variability of S^{6+}, S^{4+}, and S^{2-} in apatite as a function of oxidation state: Implications for a new oxybarometer. Am. Mineral. 102 (3), 548–557.

Konecke, B.A., Fiege, A., Simon, A.C., Linsler, S., Holtz, F., 2019. An experimental calibration of a sulfur-in-apatite oxybarometer for mafic systems. Geochim. Cosmochim. Acta 265, 242–258.

Li, X., Zhou, M., 2015. Multiple stages of hydrothermal REE remobilization recorded in fluorapatite in the Paleoproterozoic Yinachang Fe-Cu-(REE) deposit, Southwest China. Geochim. Cosmochim. Acta 166, 53–73.

Liu, Y., Hu, Z., Gao, S., Günther, D., Xu, J., Gao, C., Chen, H., 2008. *In situ* analysis of major and trace elements of anhydrous minerals by LA-ICP-MS without applying an internal standard. Chem. Geol. 257 (1–2), 34–43.

Martelat, Benoit, Isnard, Helene, Vio, Laurent, Dupuis, Erwan, Cornet, Terence, 2018. Precise U and Pu isotope ratio measurements in nuclear samples by hyphenating capillary electrophoresis and MC-ICPMS. Anal. Chem. 90 (14), 8622–8628.

Mason, P.R.D., Košler, J., de Hoog, J.C.M., Sylvester, P.J., Meffan-Main, S., Naturvetenskapliga, F., Faculty, O.S., Göteborgs, U., Institutionen, F.G., Gothenburg, U., Department, O.E.S, 2006. *In situ* determination of sulfur isotopes in sulfur-rich materials by laser ablation multiple-collector inductively coupled plasma mass spectrometry (LA-MC-ICP-MS). J. Anal. At. Spectrom. 21 (2), 177–186.

Miles, A.J., Graham, C.M., Hawkesworth, C.J., Gillespie, M.R., Hinton, R.W., Bromiley, G.D., 2014. Apatite: A new redox proxy for silicic magmas? Geochim. Cosmochim. Acta 132, 101–119.

Palma, G., Barra, F., Reich, M., Valencia, V., Simon, A.C., Vervoort, J., Leisen, M., Romero, R., 2019. Halogens, trace element concentrations, and Sr—Nd isotopes in apatite from iron oxide-apatite (IOA) deposits in the Chilean iron belt: Evidence for magmatic and hydrothermal stages of mineralization. Geochim. Cosmochim. Acta 246, 515–540.

Parat, F., Holtz, F., 2005. Sulfur partition coefficient between apatite and rhyolite: the role of bulk S content. Contrib. Mineral. Petrol. 150 (6), 643–651.

Parat, F., Holtz, F.O., 2004. Sulfur partitioning between apatite and melt and effect of sulfur on apatite solubility at oxidizing conditions. Contrib. Mineral. Petrol. 147 (2), 201–212.

Parat, F., Dungan, M.A., Streck, M.J., 2002. Anhydrite, pyrrhotite, and sulfur-rich apatite: tracing the sulfur evolution of an Oligocene andesite (Eagle Mountain, CO, USA). Lithos 64 (3), 63–75.

Parat, F., Holtz, F., Streck, M.J., 2011. Sulfur-bearing magmatic accessory minerals. Rev. Mineral. Geochem. 73 (1), 285–314.

Piccoli, P.M., Candela, P.A., Kohn, M.J., Rakovan, J., Hughes, J.M., 2002. Apatite in igneous systems. Rev. Mineral. Geochem. 48 (1), 255–292.

Rakovan, J., McDaniel, D.K., Reeder, R.J., 1997. Use of surface-controlled REE sectoral zoning in apatite from Llallagua, Bolivia, to determine a single-crystal Sm—Nd age. Earth Planet. Sci. Lett. 146 (1–2), 329–336.

Sadove, G., Konecke, B.A., Fiege, A., Simon, A.C., 2019. Structurally bound S^{2-}, S^{1-}, S^{4+}, S^{6+} in terrestrial apatite: the redox evolution of hydrothermal fluids at the Phillips mine, New York, USA. Ore Geol. Rev. 107, 1084–1096.

Sanabria-Ortega, G., Pécheyran, C., Bérail, S., Donard, O.F.X., 2012. Fast and precise method for Pb isotope ratio determination in complex matrices using GC-MC-ICPMS: application to crude oil, kerogen, and Asphaltene samples. Anal. Chem. 84 (18), 7874–7880.

Webster, J.D., Piccoli, P.M., Harlov, D.E., Rakovan, J.F., 2015. Magmatic apatite; a powerful, yet deceptive, mineral. Elements (Quebec) 11 (3), 177–182.

Yang, Y., Wu, F., Yang, J., Chew, D.M., Xie, L., Chu, Z., Zhang, Y., Huang, C., 2014. Sr and Nd isotopic compositions of apatite reference materials used in U-Th-Pb geochronology. Chem. Geol. 385, 35–55.

Yang, Z., Fryer, B.J., Longerich, H.P., Gagnon, J.E., Samson, I.M., 2011. 785 nm femtosecond laser ablation for improved precision and reduction of interferences in Sr isotope analyses using MC-ICP-MS. J. Anal. At. Spectrom. 26 (2), 341–351.

Zeng, L., Zhao, X., Li, X., Hu, H., McFarlane, C., 2016. *In situ* elemental and isotopic analysis of fluorapatite from the Taocun magnetite-Apatite deposit, Eastern China: constraints on fluid metasomatism. Am. Mineral. 101 (11), 2468–2483.

Zhang, W., Hu, Z., 2020. A critical review of isotopic fractionation and interference correction methods for isotope ratio measurements by laser ablation multi-collector inductively coupled plasma mass spectrometry. Spectrochim. Acta B At. Spectrosc. 171, 105929.

Zhang, W., Hu, Z., Liu, Y., 2020. Iso-Compass: new freeware software for isotopic data reduction of LA-MC-ICP-MS. J. Anal. At. Spectrom. 35 (6), 1087–1096.

Zhu, Z., Jiang, S., Ciobanu, C.L., Yang, T., Cook, N.J., 2017. Sulfur isotope fractionation in pyrite during laser ablation: implications for laser ablation multiple collector inductively coupled plasma mass spectrometry mapping. Chem. Geol. 450, 223–234.

Zirner, A.L.K., Marks, M.A.W., Wenzel, T., Jacob, D.E., Markl, G., 2015. Rare earth elements in apatite as a monitor of magmatic and metasomatic processes: The Ilímaussaq complex, South Greenland. Lithos 228–229, 12–22.